Electronic Supplementary Information (ESI)

Advanced Core-Shell Hollow Carbon Nanofibers for Ion and Electron Accessibility in Sodium Ion Batteries

Zhisong He [a], Yu Liu [a], Xiaozhi Yuan [a], Xijun Wei [a*], Shibo Liu [a], Yang Cao [a], Changrui Lu [a], Zhixin Wang [a], Bo Zhao [a], Qi Wan [a*] and Yingze Song [a*]

[a] State Key Laboratory of Environment-Friendly Energy Materials, Engineering Research Center of Biomass Materials, Ministry of Education, School of Materials and Chemistry, Southwest University of Science and Technology, Mianyang, Sichuan 621010, China.

Corresponding authors: xijunwei1992@swust.edu.cn (X. Wei), yzsong@swust.edu.cn (Y. Song).

Keywords: hollow carbon nanofibers, core-shell structure, hard carbon material, sodium storage

1. Experimental Section

1.1 Synthesis of CA fibrous membranes

The 18 *wt.%* cellulose acetate (CA) powder was dissolved in a cosolvent of acetone (AC) and N, N-dimethylformamide (DMF) (1:1 = w: w) and stirred at 30 ℃ for 12 h to form a uniform CA spinning solution. Then, the CA spinning solution was transferred to a 10 ml syringe and single axis electrospinning was carried out at a high pressure of 14 kV. The process parameters of electrospinning were as follows: the distance between collector and needle was 15 cm, the needle size was 23 G, the humidity was 40%, and the advance rate was 1 ml h^{-1}. Finally, the CA fibrous membranes collected from the roller was dried in a vacuum drying oven at 60 ℃ for 8 h to remove the residual solvent.

1.2 Synthesis of PAN fibrous membranes

The 10 *wt.%* polyacrylonitrile (PAN) powder was dissolved in DMF solvent and stirred at 60 ℃ for 6 h to form a uniform PAN spinning solution. Under the same conditions, the PAN fibrous membranes were prepared by single axis electrospinning and drying.

1.3 Synthesis of CA@PAN core-shell composite fibrous membranes

The CA spinning solution was used as the core solution and the PAN spinning solution as the shell solution. The core and shell solution were loaded into two 10 ml syringes and connected to the inner nozzle and outer nozzle of the coaxial nozzle instrument (23 G–17 G) respectively. Compared with the outer nozzle, the end of the inner nozzle was adjusted to the outward direction by 1 mm. Coaxial electrospinning process parameters were as follows: applied voltage 11–13 kV, injection flow rate of inner and outer nozzles was 0.5 ml h^{-1} and 1 ml h^{-1} respectively, humidity was 30%, the fiber film collected from the roller was dried under the same conditions to obtain CA@PAN core-shell composite fibrous membranes.

1.4 Synthesis of CA-CNFs、PAN-CNFs、HCNFs

Firstly, the dried CA, PAN and CA@PAN fibrous membranes were soaked in 0.1 M mixture of NaOH and C_2H_5OH solution for 24 h, and then washed with deionized water to remove excess lye. Then, the obtained CA, PAN and CA@PAN fibrous membranes were carbonized, heated to 260 ℃ at a heating rate of 2 ℃ min^{-1}, and pre-oxidized for

2 h. Then, under the protection of Ar, it was heated to 900 ℃ at a heating rate of 5 ℃ min^{-1}, and carbonized for 3 h. Finally, CA-CNFs, PAN-CNFs, HCNFs were obtained.

2. Characterization

The crystal structure, grain size and lattice constant of the materials were characterized by X-ray diffractometer (XRD, Bruker D Advance) at a scanning rate of 10° min^{-1} under Cu Kα radiation. The morphology and microstructure of the materials were characterized by scanning electron microscopy (SEM, JSM-7800F) and transmission electron microscopy (TEM, JEM-2000EX). The structure of carbon in the material was characterized by Raman spectrometer (Renishaw inVia). The weight content of the material was determined by thermogravimetric analysis (TGA, NETZSCH TG 209F1) under the condition of 50 to 800 ℃ and nitrogen heating rate of 10 ℃ min^{-1}. The specific surface area (SSA) and porous structure of the material were measured using a Brunauer-Emmett-Teller (BET) and Barrett-Joyner-Halenda (BJH) methods based on N_2 adsorption-desorption isotherms tested on Micromeritics Tristar3000 at 77 K. The X-ray Photoelectron Spectroscopy (XPS, Thermo Scientific K-Alpha) was used to detect the element composition and valence distribution on the surface of the material, and the proportion of each element was obtained through subsequent calculation.

3. Electrochemical Measurement

The active material, the conductive agent (carbon black) and the binder (polyvinylidene fluoride, PVDF) were mixed in 1-methyl-2-pyrrolidinone (NMP) solvent at a weight ratio of 8:1:1 to form a uniform slurry, and then the slurry was coated on a Cu foil current collector to prepare the working electrode. After drying in a vacuum drying oven at 60 ℃ for 24 h, the working electrode was cut into a disk electrode with a diameter of 13 mm. Assemble the CR2032 half cell in a glove box filled with high purity argon gas (H_2O < 0.01 ppm, O_2 < 0.01 ppm). These include a positive shell, a working electrode, a fiberglass diaphragm (Whatman, Grade GF/D), an electrolyte (1.0 M $NaPF_6$ in diglyme), metallic sodium, gaskets, shrapnel and a negative shell. The constant current charge-discharge cycle experiment of half battery was carried out in NEWARE battery test system with voltage range of 0.01–3 V. Electrochemical

impedance spectroscopy (EIS) was conducted with an AC voltage amplitude of 5 mV in a frequency range of 0.01 Hz–100 kHz at an open circuit potential. Cyclic voltammetry (CV) curves were obtained by LAND battery system at different scanning rates. To further investigate the kinetic properties of Na^+, the galvanostatic intermittent titration technique (GITT) was used to test at A current density of 0.1 A g^{-1}, where the pulse time was 10 mins and the rest time was 30 mins, and then discharged in the same manner.

4. Figures

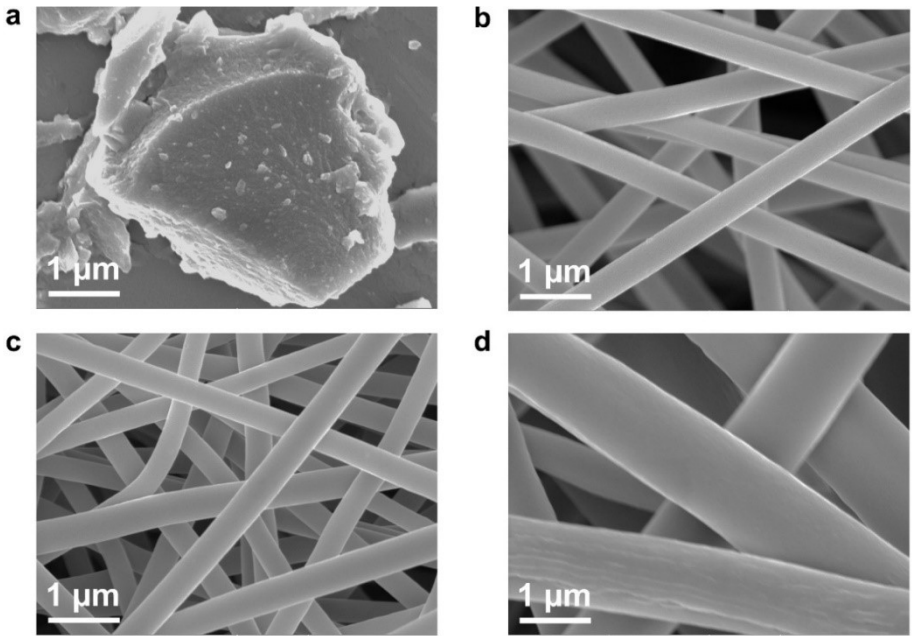

Fig. S1 (a) SEM image of CA-CNFs without deacetylation, SEM images of (b) CA-CNFs, (c) PAN-CNFs, (d) HCNFs after deacetylation.

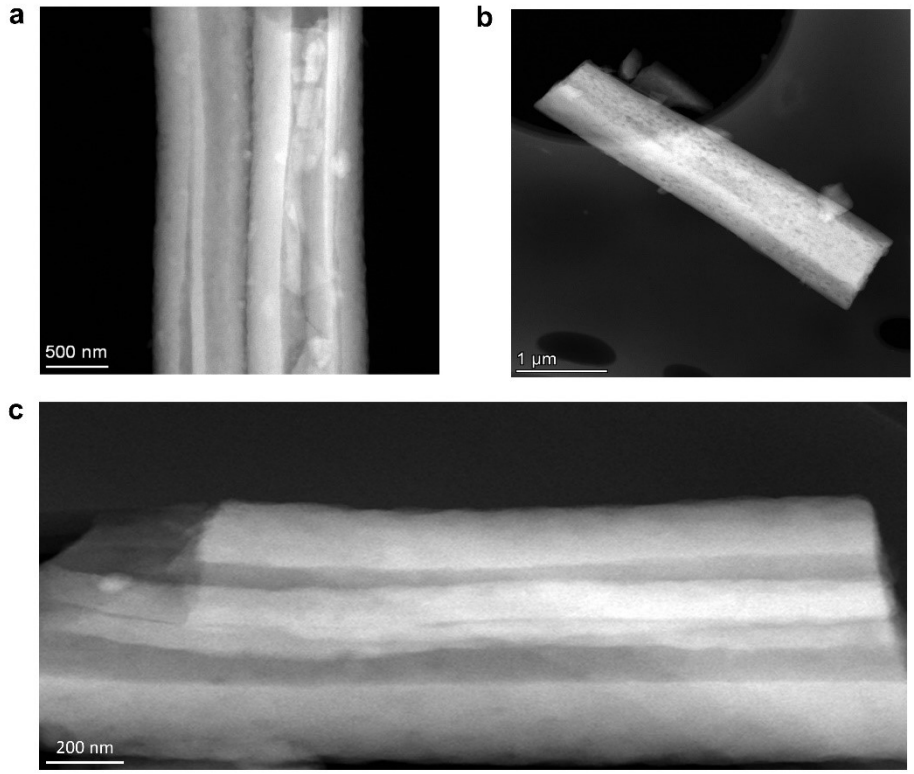

Fig. S2 (a-c) TEM images of HCNFs.

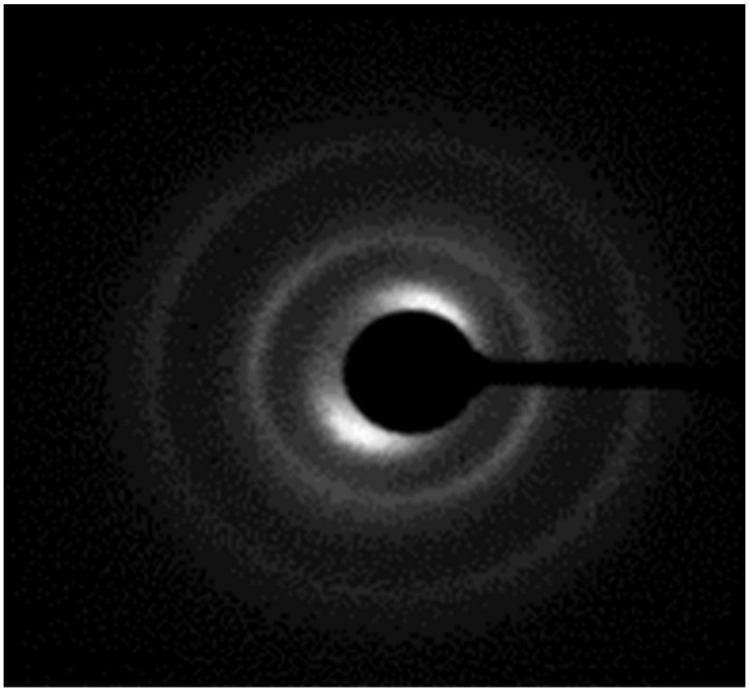

Fig. S3 SAED image of HCNFs shell.

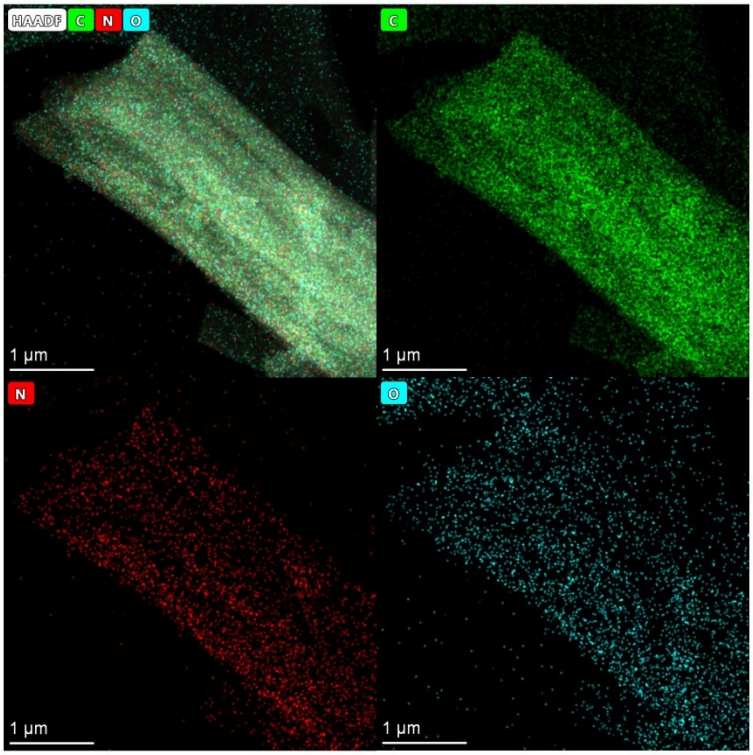

Fig. S4 EDS elemental mapping images for HCNFs.

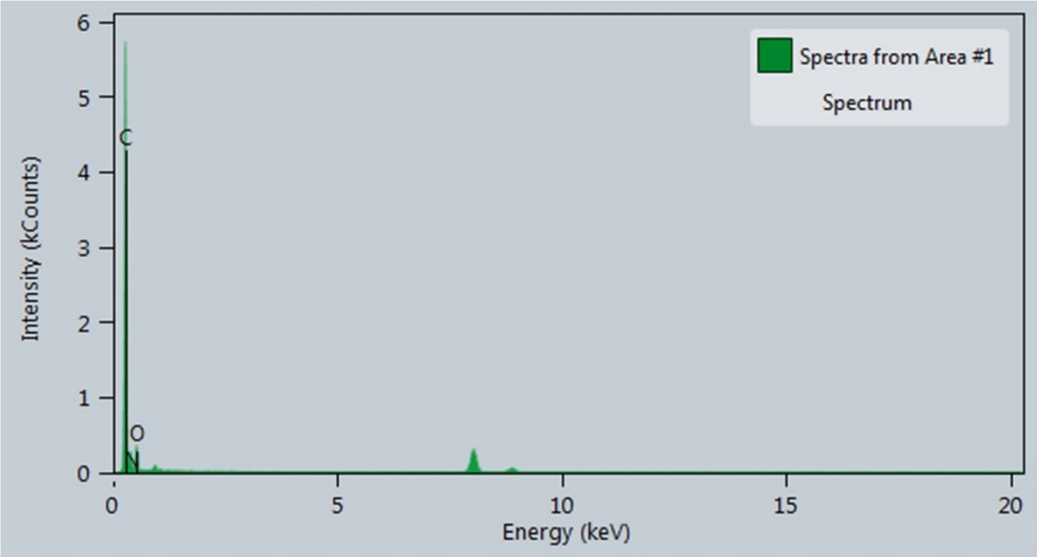

Fig. S5 EDS spectra of HCNFs.

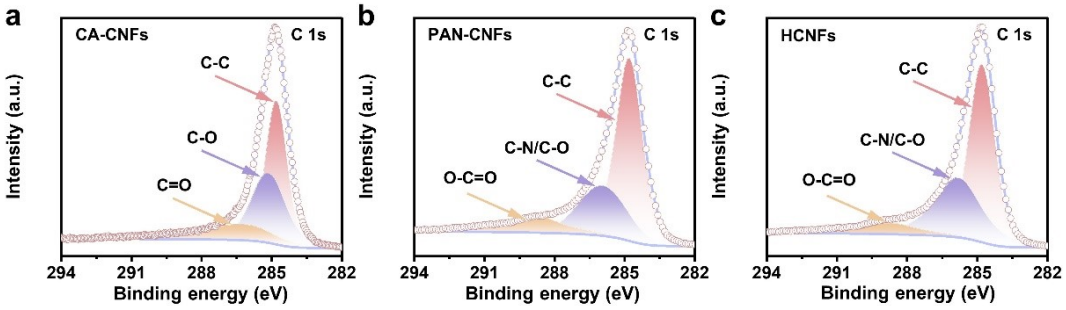

Fig. S6 High-resolution C 1s spectra of (a) CA-CNFs, (b) PAN-CNFs, (c) HCNFs.

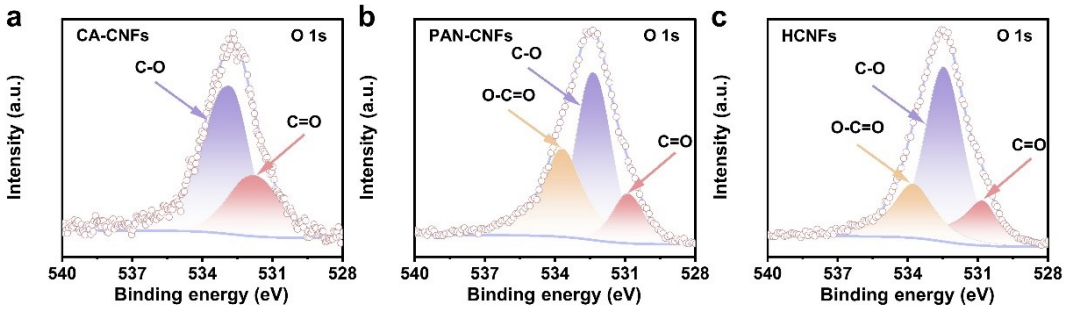

Fig. S7 High-resolution O 1s spectra of (a) CA-CNFs, (b) PAN-CNFs, (c) HCNFs.

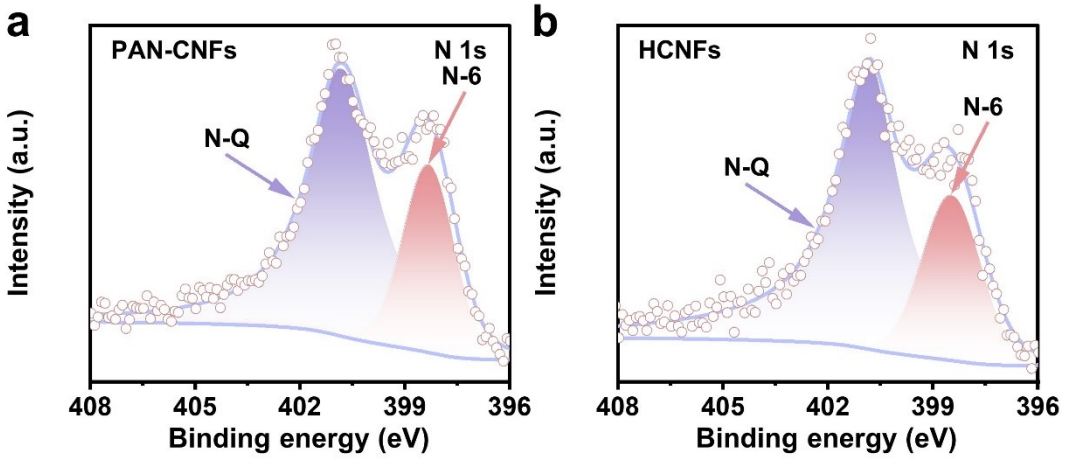

Fig. S8 High-resolution N 1s spectra of (a) PAN-CNFs, (b) HCNFs.

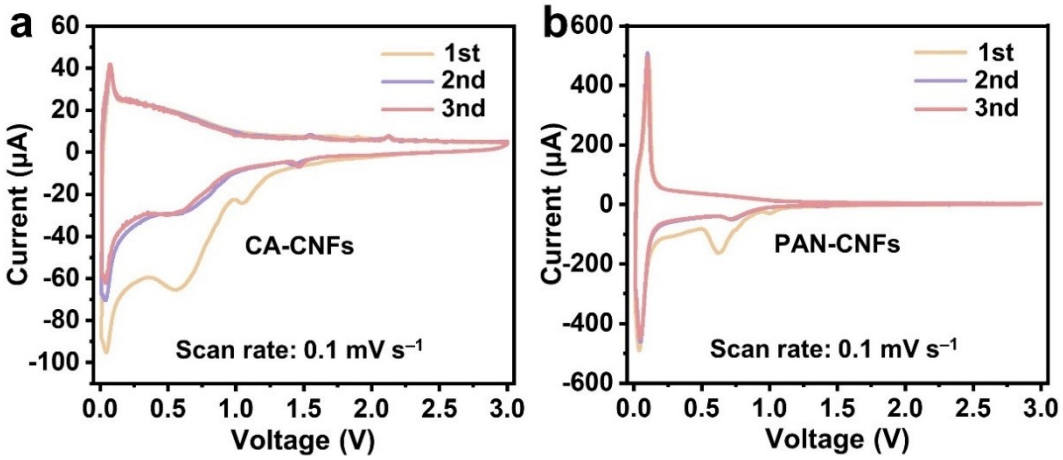

Fig. S9 CV curves of the (a) CA-CNFs, (b) PAN-CNFs anode at the scan rate of 0.1 mV s^{-1}.

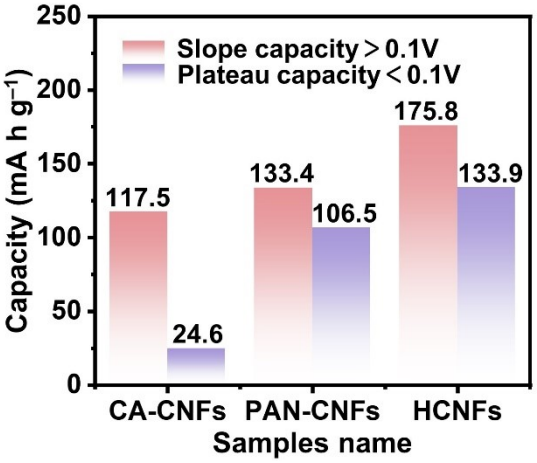

Fig. S10 Capacity distribution at different potential regions based on the first GCD curves.

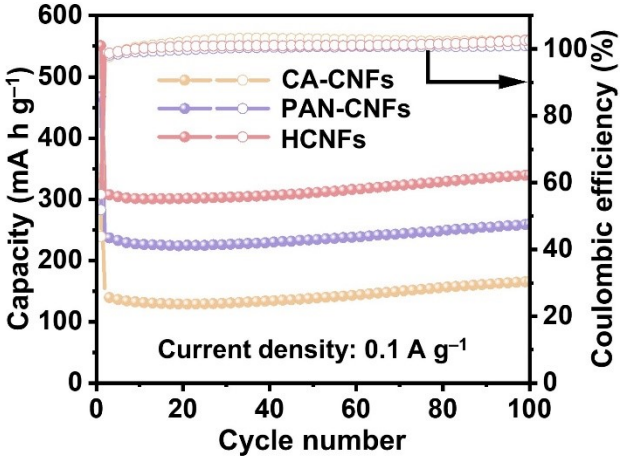

Fig. S11 Cycling performance of CA-CNFs, PAN-CNFs and HCNFs at 0.1 A g^{-1}.

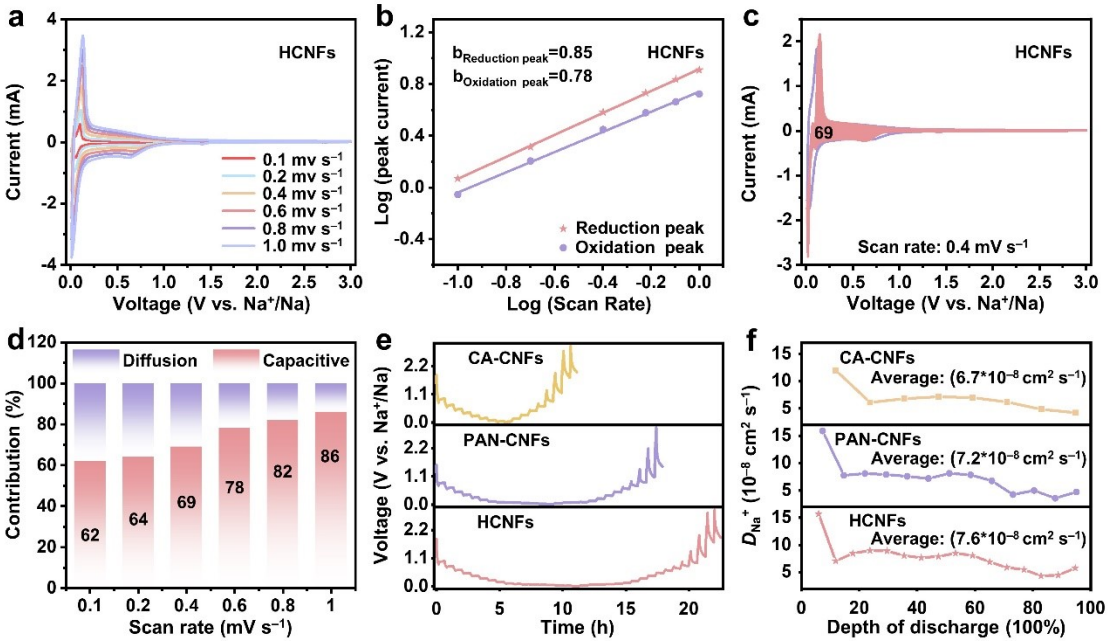

Fig. S12 (a) CV curves of HCNFs electrode at different scan rates. (b) b value calculation according to the relationship between peak current and scan rate of HCNFs. (c) The capacitive contribution of HCNFs at 0.4 mV s^{-1}. (d) Histograms of the capacity contribution of HCNFs at different scan rates. (e) GITT potential profiles of CA-CNFs, PAN-CNFs and HCNFs. (f) Obtained Na^+ diffusion coefficient variation graph of CA-CNFs, PAN-CNFs and HCNFs.

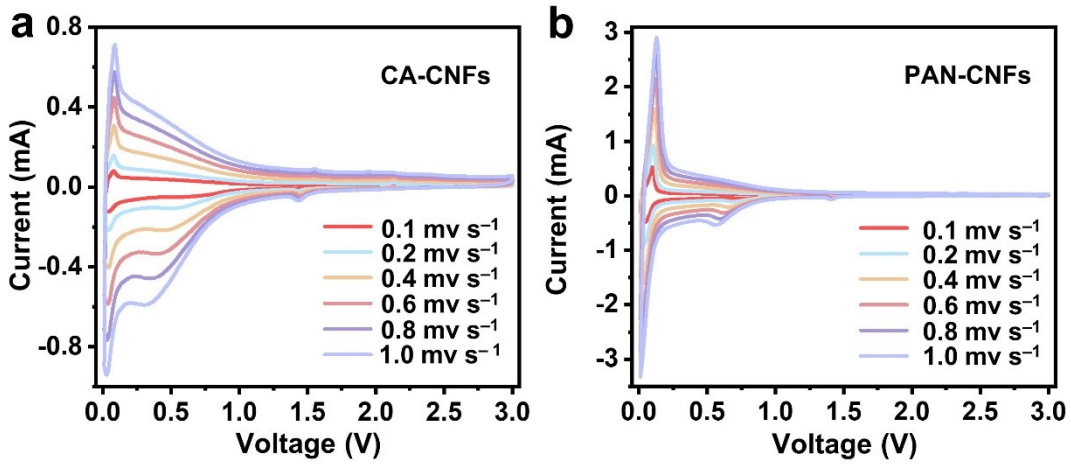

Fig. S13 CV curves of (a) CA-CNFs, (b) PAN-CNFs electrode at different scan rates.

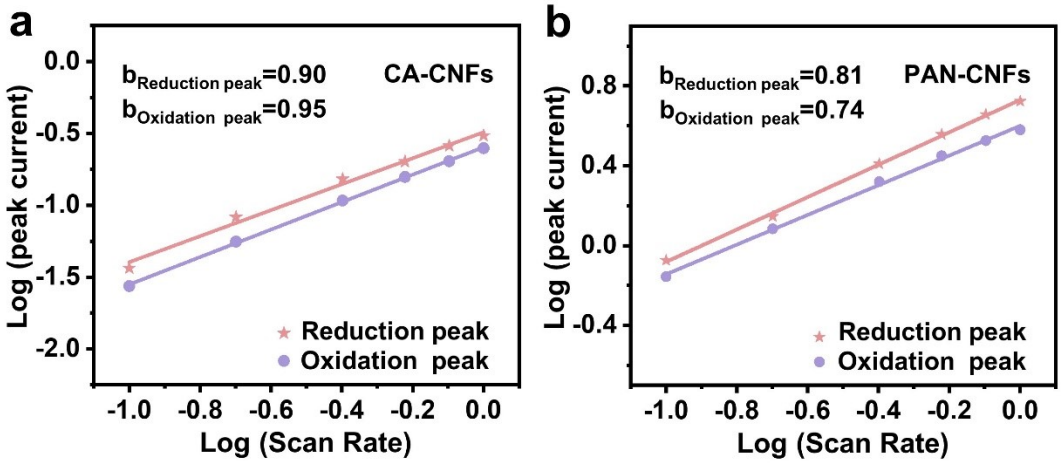

Fig. S14 b-value calculation according to the relationship between peak current and scan rate of (a) CA-CNFs, (b) PAN-CNFs.

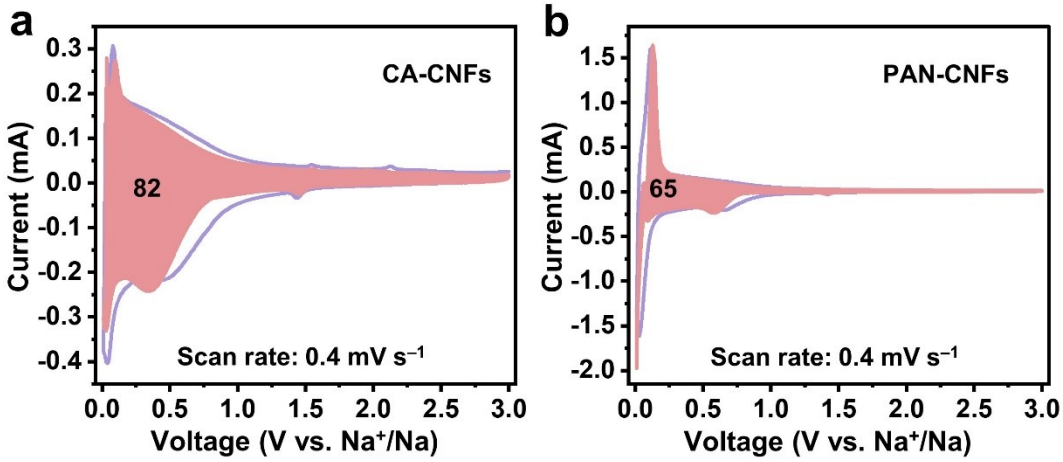

Fig. S15 The capacitive contribution of (a) CA-CNFs, (b) PAN-CNFs at 0.4 mV s^{-1}.

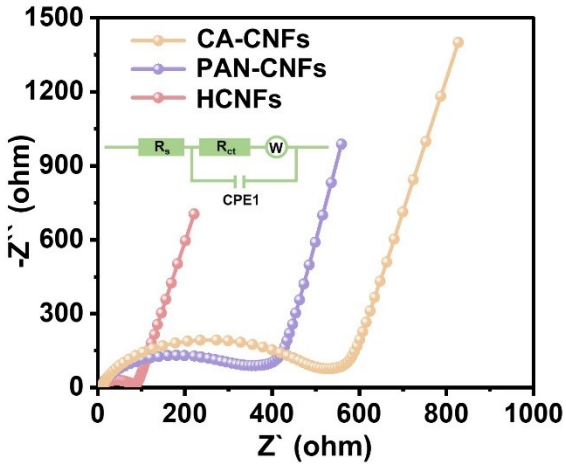

Fig. S16 EIS spectra of CA-CNFs, PAN-CNFs and HCNFs (the inset show the corresponding electric equivalent circuits).

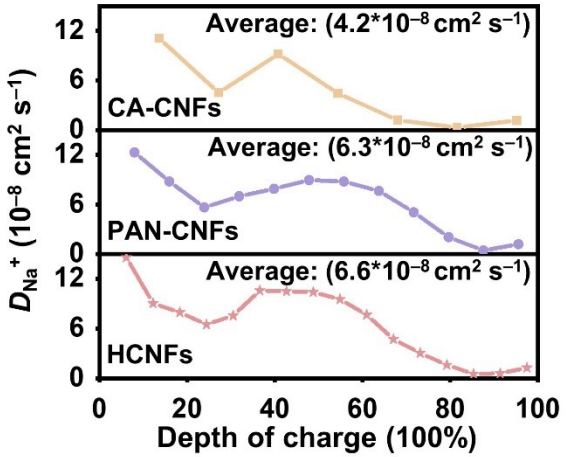

Fig. S17 The sodium-ion diffusion coefficient variation graph of CA-CNFs, PAN-CNFs and HCNFs during charging.

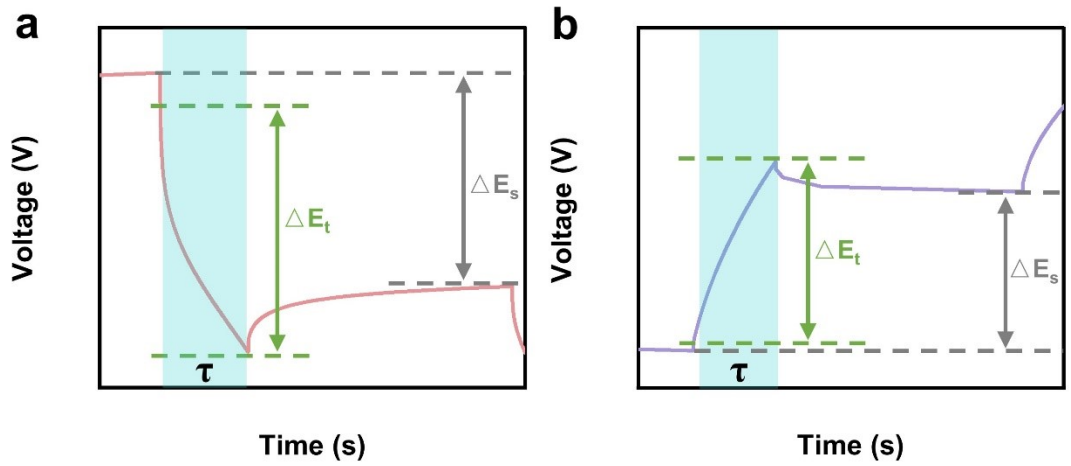

Fig. S18 Schematic representation of the GITT in discharge process. Note: The diffusion coefficients are calculated using Fick's second law with the following Equation (Where τ means the duration of the current pulse, L is electrode thickness. Besides, τ, ΔE_s and ΔE_t could be obtained from the GITT curves.)

$$D_k = \frac{4L^2 \Delta E_S^{\,2}}{\pi\tau\ \Delta E_t^{\,2}}$$

Table S1. Elemental analysis results of the as-prepared CA-CNFs, PAN-CNFs and HCNFs.

Samples	C	O	N
CA-CNFs	**92.84**	**7.16**	**-**
PAN-CNFs	**84.09**	**9.32**	**6.59**
HCNFs	**84.08**	**9.63**	**6.29**

Table S2. Comparison of electrochemical properties of HCNFs with other carbon-based materials

Ref.	Sample	Cycle number	Specific capacity
This work	**HCNFs**	**100 cycles**	**310 mA h g^{-1} at 0.1 A g^{-1}**
		500 cycles	**220 mA h g^{-1} at 2 A g^{-1}**
[1]	**MnO_2 NSs@CNFs-1%**	**500 cycles**	**175.1 mA h g^{-1} at 0.5 A g^{-1}**
[2]	**3D PCN**	**200 cycles**	**266 mA h g^{-1} at 0.1 A g^{-1}**
		200 cycles	**184 mA h g^{-1} at 0.5 A g^{-1}**
[3]	**HCNF**	**100 cycles**	**276 mA h g^{-1} at 0.1 A g^{-1}**
[4]	**PN-CFs-700**	**600 cycles**	**170.5 mA h g^{-1} at 0.2 A g^{-1}**
[5]	**MoO_2@HCNF**	**500 cycles**	**221.55 mA h g^{-1} at 0.2 A g^{-1}**
[6]	**SNCNF**	**100 cycles**	**290.3 mA h g^{-1} at 0.1 A g^{-1}**
[7]	**CNF@CDs-0.2**	**400 cycles**	**214.08 mA h g^{-1} at 0.02 A g^{-1}**
		400 cycles	**196.1 mA h g^{-1} at 0.1 A g^{-1}**
[8]	**CNF@NPC**	**100 cycles**	**240 mA h g^{-1} at 0.1 A g^{-1}**
		400 cycles	**148.8 mA h g^{-1} at 0.5 A g^{-1}**
[9]	**PAN-CNFs-1250**	**100 cycles**	**275 mA h g^{-1} at 0.02 A g^{-1}**
[10]	**HPCCNFs-1**	**100 cycles**	**215 mA h g^{-1} at 0.1 A g^{-1}**
		1000 cycles	**109 mA h g^{-1} at 5 A g^{-1}**
[11]	**S-NCNF**	**100 cycles**	**336.2 mA h g^{-1} at 0.05 A g^{-1}**
		2000 cycles	**187 mA h g^{-1} at 2 A g^{-1}**
[12]	**NCNFs-IWNC800**	**350 cycles**	**278 mA h g^{-1} at 0.1 A g^{-1}**

Table S3. The EIS fitting parameters of CA-CNFs, PAN-CNFs and HCNFs.

Samples	R_s (Ω)	R_{ct} (Ω)
CA-CNFs	**8.5**	**471.9**
PAN-CNFs	**6.2**	**310.5**
HCNFs	**5.6**	**70.2**

Table S4. Diffusion coefficient of CA-CNFs, PAN-CNFs and HCNFs electrodes.

CA-CNFs Discharge	CA-CNFs Charge	PAN-CNFs Discharge	PAN-CNFs Charge	HCNFs Discharge	HCNFs Charge
1.19×10^{-7}	1.11×10^{-7}	1.59×10^{-7}	1.23×10^{-7}	1.57×10^{-7}	1.46×10^{-7}
6.1×10^{-8}	4.51×10^{-8}	7.76×10^{-8}	8.78×10^{-8}	7.06×10^{-8}	9.05×10^{-8}
6.8×10^{-8}	7.19×10^{-8}	8.09×10^{-8}	5.66×10^{-8}	8.45×10^{-8}	7.95×10^{-8}
7.15×10^{-8}	4.44×10^{-8}	7.92×10^{-8}	7×10^{-8}	8.98×10^{-8}	6.5×10^{-8}
6.99×10^{-8}	1.19×10^{-8}	7.58×10^{-8}	7.9×10^{-8}	8.89×10^{-8}	7.57×10^{-8}
6.18×10^{-8}	3.12×10^{-9}	7.18×10^{-8}	8.95×10^{-8}	8.04×10^{-8}	1.06×10^{-7}
4.84×10^{-8}	1.17×10^{-8}	8.12×10^{-8}	8.79×10^{-8}	7.66×10^{-8}	1.05×10^{-7}
4.23×10^{-8}		7.86×10^{-8}	7.65×10^{-8}	7.89×10^{-8}	1.04×10^{-7}
		6.75×10^{-8}	5.07×10^{-8}	8.48×10^{-8}	9.53×10^{-8}
		4.24×10^{-8}	2.06×10^{-8}	8.07×10^{-8}	7.67×10^{-8}
		4.98×10^{-8}	4.59×10^{-9}	6.89×10^{-8}	4.71×10^{-8}
		3.57×10^{-8}	1.21×10^{-8}	5.87×10^{-8}	3.03×10^{-8}
		4.71×10^{-8}		5.48×10^{-8}	1.6×10^{-8}
				4.34×10^{-8}	5.08×10^{-9}
				4.46×10^{-8}	5.86×10^{-9}
				5.77×10^{-8}	1.27×10^{-8}
Average diffusion coefficient (D_k)					
6.77×10^{-8}	4.27×10^{-8}	7.28×10^{-8}	6.31×10^{-8}	7.63×10^{-8}	6.63×10^{-8}

References

1 S. Zheng, D. Li, W. Li, J. Chen, X. Rao, N. Wang, J. Qi, B. Wang, S. Luo and Y. Zhao, *ACS Appl. Energy Mater.*, 2022, **5**, 3587-3594.

2 Q. Zhang, Y. Zhang, S. Liu and H. Yang, *Appl. Clay. Sci.*, 2021, **200**, 105916.

3 H. Han, X. Chen, J. Qian, F. Zhong, X. Feng, W. Chen, X. Ai, H. Yang and Y. Cao, *Nanoscale*, 2019, **11**, 21999-22005.

4 K. Xue, Y. Si, S. Xie, J. Yang, Y. Mo, B. Long, W. Wei, P. Cao, H. Wei, H. Guan, E. G. Michaelis, G. Guo, Y. Yue and C. Shan, *Front. Chem.*, 2021, **9**, 647545.

5 N. Feng, M. Gao, J. Zhong, C. Gu, Y. Zhang and B. Liu, *Polymers*, 2024, **16**, 1452.

6 M. Yu, Z. Yin, G. Yan, Z. Wang, H. Guo, G. Li, Y. Liu, L. Li and J. Wang, *J. Power Sources*, 2020, **449**, 227514.

7 H. Guo, X. Qu, B. Xing, H. Zeng, W. Kang, S. Cheng, Y. Xing, J. He and C. Zhang, *Appl. Surf. Sci.*, 2024, **660**, 159999.

8 Z. Zhang, J. Zhang, X. Zhao and F. Yang, *Carbon*, 2015, **95**, 552-559.

9 J. Jin, Z. Shi and C. Wang, *Electrochim. Acta*, 2014, **141**, 302-310.

10 J. Gao, X. Wang, X. Lu, C. Chao, Y. Liang, P. Gao, Y. Sun, A. Liu and Y. Huang, *ChemElectroChem*, 2022, **9**, e202200496.

11 X. Sun, C. Wang, Y. Gong, L. Gu, Q. Chen and Y. Yu, *Small*, 2018, **14**, e1802218.

12 W. Zhao, X. Hu, S. Ci, J. Chen, G. Wang, Q. Xu and Z. Wen, *Small*, 2019, **15**, e1904054.